communications earth & environment

A Nature Portfolio journal

Article

https://doi.org/10.1038/s43247-025-03154-8

Measurement of a lithium plume from the uncontrolled re-entry of a Falcon 9 rocket

Check for updates

Robin Wing[1,5] ✉, **Michael Gerding**[1,5], **John M. C. Plane**[2,5], **Yanmichel A. Morfa**[1,5], **J. Miguel Urco**[1,3,5], **Yosuke Yamazaki**[1,5], **Leonard Schulz**[4,5], **Josef Höffner**[1,5], **Jens Mielich**[1,5], **Toralf Renkwitz**[1,5], **Claudia C. Stephan**[1,5], **Gerd Baumgarten**[1,5] & **Claudia Stolle**[1,5]

A 10-fold enhancement of lithium atoms was detected at 96 km altitude by a resonance lidar at Kühlungsborn, Germany, approximately 20 hours after the uncontrolled re-entry of a Falcon 9 upper stage. The upper-atmospheric extension of the ICON general circulation model, nudged to ECMWF, was used to calculate winds. Backwards trajectories, including wind variability as measured by radar, traced air masses to the Falcon 9 re-entry path at 100 km altitude, west of Ireland. This study presents the first measurement of upper-atmospheric pollution resulting from space debris re-entry and the first observational evidence that the ablation of space debris can be detected by ground-based lidar. The analysis of geomagnetic conditions, atmospheric dynamics, and ionospheric measurements supports the claim that the enhancement was not of natural origin. Our findings demonstrate that identifying pollutants and tracing them to their sources is achievable, with significant implications for monitoring and mitigating space emissions in the atmosphere.

The increasing frequency of satellite and rocket re-entries is an emerging societal and scientific concern. While the risks to people and infrastructure from falling debris are widely discussed, less attention has been paid to the environmental consequences for Earth's atmosphere. In particular, the upper atmosphere is now subject to the injection of exotic atomic and molecular species not typically found in large quantities in natural meteoric input. Between 03:44 and 03:52 UTC on 19 February 2025, the upper stage of a SpaceX Falcon 9 rocket made an uncontrolled re-entry over Europe, producing a visible fireball and a persistent high-altitude plume of lithium vapour. This event provides a rare opportunity to examine the upper atmospheric signature of space debris re-entry using a suite of advanced remote sensing instruments and atmospheric models. Here we show that this re-entry event injected sufficient atomic lithium into the Mesosphere and Lower Thermosphere (MLT) that the plume was detectable over Northern Germany, having advected approximately 1600 km, from the west coast of Ireland over approximately 20 hours. This is the first observation of MLT pollution by re-entering space debris made by a lidar, and the first use of the upper-atmospheric extension of the Icosahedral Nonhydrostatic circulation model (UA-ICON) winds to calculate back trajectories in the upper atmosphere. It also represents the first observational evidence that the ablation process begins as high as 100 km altitude. This finding supports growing concerns that space traffic may pollute the upper atmosphere in ways not yet fully understood. Continued growth in satellite launches and re-entries may lead to cumulative effects, with implications for long-term atmospheric composition and climate interactions.

The so-called "New Space Age" is characterised by the rapid deployment of commercial mega-constellations in low Earth orbit (LEO) consisting of tens of thousands of satellites. This development represents not only a dramatic increase in satellite numbers but also a significant rise in total orbital mass.

For example, the Starlink constellation is planned to consist of over 40,000 satellites, each with a mass of between 305 and 960 kg, yielding a cumulative mass exceeding 10,000 tonnes[1]. Given their typical operational lifetimes of five years and the NASA/ESA requirements for deorbiting satellites after their regular use, these satellites are expected to re-enter Earth's atmosphere through uncontrolled decay within the next several years. The serendipitous measurement of the Falcon 9 decomposition presented in this case study exemplifies what is expected to happen going forward, as some fraction of mega-constellation satellites re-enter the atmosphere each day.

Projections suggest that within the next decades, the mass flux from artificial satellite re-entries could exceed 40% of the natural meteoroid

---

[1]Leibniz Institute of Atmospheric Physics, Schloßstraße 6, Kühlungsborn, 18225, Germany. [2]School of Chemistry, University of Leeds, Woodhouse Lane, Leeds, LS2 9JT, UK. [3]Departamento de Ingeniería, Pontificia Universidad Católica del Perú, 1801 Universitaria Avenue, Lima, 15088, Peru. [4]Institute of Geophysics and Extraterrestrial Physics, Technische Universität Braunschweig, Mendelssohnstr. 3, Braunschweig, 38106, Germany. [5]These authors contributed equally: Robin Wing, Michael Gerding, John M. C. Plane, Yanmichel A. Morfa, J. Miguel Urco, Yosuke Yamazaki, Leonard Schulz, Josef Höffner, Jens Mielich, Toralf Renkwitz, Claudia C. Stephan, Gerd Baumgarten, Claudia Stolle. ✉e-mail: wing@iap-kborn.de

influx[2]. However, the significance of this trend lies not only in the increasing total mass but also in the compositional differences between natural meteoroids and re-entering spacecraft. Unlike the elemental composition of chondritic meteoroids[3], satellites, and rocket stages introduce engineered materials such as aluminium alloys, composite structures, and rare earth elements from onboard electronics, substances rarely found in natural extraterrestrial matter[4].

Despite the important role Earth's upper atmosphere plays in shielding terrestrial life, the consequences of increasing pollution from re-entering space debris on radiative transfer, ozone chemistry[5], and aerosol microphysics remain largely unknown[6,7]. Recent aircraft-based measurements have already detected signatures of space-debris-derived material in the stratosphere, with approximately 10% of sulphuric-acid particles larger than 120 nm containing metals in ratios consistent with spacecraft alloys[8]. Whole-atmosphere and process-resolving modelling indicates that alumina and co-emitted metals from re-entry can accumulate and persist for years, with injections expected to grow as re-entry frequency increases; these burdens may perturb stratospheric ozone, aerosol size-composition distributions through alumina and other metal-oxide formation, temperatures, winds, and radiative balance[5,7,9]. Of particular concern are metal elements not highly abundant in meteoroids, which may introduce novel pathways for heterogeneous chemistry, aerosol nucleation, and catalytic ozone depletion. The potential influence of these metals on the formation and radiative properties of stratospheric and mesospheric aerosols, including polar stratospheric clouds, represents a critical knowledge gap. This gap limits our understanding of how anthropogenic materials may perturb climate-relevant processes operating in the upper atmosphere[7,10], and it motivates the present event-scale observations as an essential constraint on emission inventories, altitude-time ablation profiles, and chemical pathways[5,7–9]. These processes and their interactions are summarised schematically in Fig. 1.

Why measure lithium?

Metals such as aluminium (Al), copper (Cu), lithium (Li), titanium (Ti), niobium (Nb), molybdenum (Mo), silver (Ag), tin (Sn), hafnium (Hf), and lead (Pb) are considered effective tracers of space debris pollution. These elements are commonly used in aerospace components, but are not typically abundant in natural meteoroids[8]. In contrast, elements such as sodium (Na), magnesium (Mg), potassium (K), chromium (Cr), iron (Fe), and nickel (Ni) are either not present in significant quantities in spacecraft, or occur in both anthropogenic and meteoric sources, making them more ambiguous as indicators of artificial material input into the atmosphere.

Lithium was selected as the initial target metal for detecting space debris signatures due to its ultra-trace abundance in chondritic meteoroids[4] and its well-documented applications in spacecraft, including lithium-ion batteries and lithium-aluminium (Li-Al) alloy hull plating[1,2]. Lithium vaporises quickly during the ablation of a Li-Al structure, appearing in the atmosphere as the aluminium matrix melts at 933 K. Using the Leeds Chemical Ablation Model[11], we derive estimates for the altitudes at which an Al-Li hull will begin to melt (see Methods in Sect. 5). For the hull thickness of the Falcon 9, 4.7 mm, melting and vaporisation of lithium is expected to begin at approximately 98.2 km.

The strong atomic resonance fluorescence line of lithium at 670.7926 nm (air) enables the detection by lidar of very trace amounts of lithium in the MLT[12], allowing altitude- and time-resolved measurements of lithium number density during and after re-entry events.

The chondritic Li/Na elemental abundance ratio is 9.8×10^{-4} [13]. The daily injection rate of Na is estimated to be 0.27 tons day^{-1} [14]. Assuming Li and Na ablate with similar efficiencies from cosmic dust particles entering the atmosphere, the estimated natural Li input is 80 grams per day. A single Falcon 9 upper stage is estimated to contain about 30 kg of lithium from the Al-Li AA 2198 alloy used in the tank walls[15]. The large disparity between the natural meteoric lithium influx and the lithium content of a single rocket stage makes lithium a sensitive tracer of anthropogenic inputs from space debris re-entries.

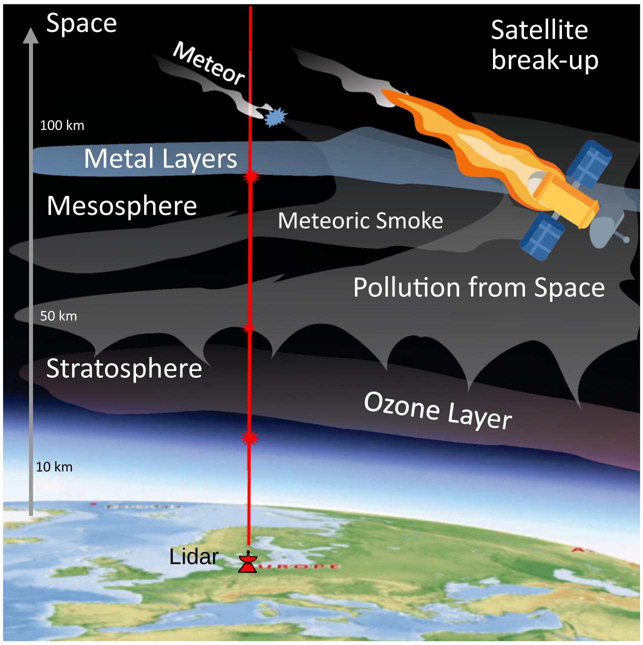

Fig. 1 | A schematic overview for the measurement of pollution from space. Natural metal layers form in the upper mesosphere due to meteor ablation and are measured by lidar. Additional mass and elements are now being introduced via the burn-up of artificial satellites. This new type of pollution has unknown consequences for the upper atmosphere and ozone layer.

Results

Falcon 9 uncontrolled re-entry

The Falcon 9 upper stage re-entered Earth's atmosphere on 19 February 2025, around 03:42 UTC, at an altitude of ~ 100 km, off the western coast of Ireland (52°N, 12°W). The re-entry produced a spectacular fireball as the stage disintegrated over Central Europe and was observed by numerous people, cameras, and radar systems between about 3:44 and 3:52 UTC. The event garnered international attention when debris fragments, including a fuel tank, were recovered near the Polish city of Poznań.

Observational and modelling overview

This study employs a suite of observational and modelling techniques to investigate lithium number density, atmospheric circulation, geomagnetic activity, and rocket ablation. Mesospheric lithium is detected by a resonance fluorescence lidar in Kühlungsborn (54°N, 12°E). Local mesospheric dynamics were obtained from the SIMONe Germany meteor radar, while global circulation was provided by the Upper Atmosphere ICON (UA-ICON) model. Sporadic E activity was monitored with ionosonde data from Juliusruh (55°N, 13°E), geomagnetic variations were quantified using a local K-index, and the Leeds Chemical Ablation Model was applied to simulate the re-entry ablation of the Falcon 9 rocket stage. A full accounting of each observational and modelling tool is available in Sect. "Methods".

Measurement of a lithium plume by lidar

The resonance fluorescence lidar operated for six hours on the night of 19-20 February, measuring lithium atom number density profiles. The peak lithium layer density was below 3 atoms cm^{-3} during most of the measurement. A sudden increase in signal by a factor of 10 was detected just after midnight UTC on 20 February (see Fig. 2). The plume appeared at 00:21 UTC and was detected for a total duration of about 40 minutes and persisted until the end of the sounding. The plume was tightly confined in altitude, with sharply defined boundaries between 94.5 and 96.8 km, and was observed until the end of the lidar operation. Lidar operation ceased at 00:48 UTC when the supply of prepared laser dye was exhausted.

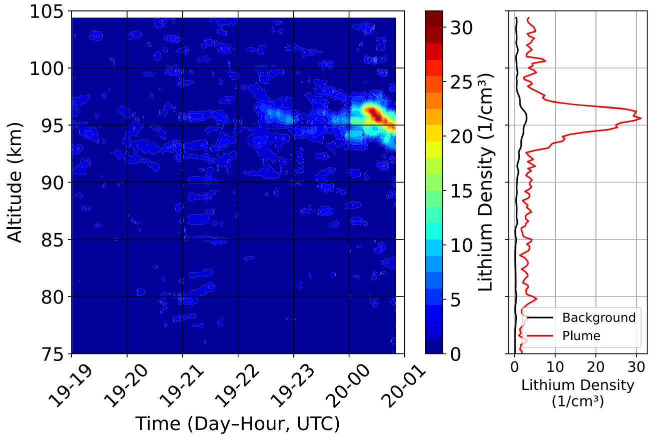

Fig. 2 | Measurement of lithium plume by lidar. Lithium observation on the night of 19/20 February 2025. Maximum lithium density before the plume arrival (2025-02-19 19:00 to 2025-02-20 00:21 UTC) is 3.0 ± 1.1 atoms cm^{-3}, observed at about 96 km. The maximum lithium density observed in the plume is 31 ± 8.3 atoms cm^{-3}, recorded at 2025-02-20 00:30 UTC at an altitude of 96.1 km. The plume has a vertical extent from 94.5 to 96.8 km, and lasted from just after midnight UTC to the end of lidar operations at 00:48 UTC. The vertical grid spacing is Δ_z = 200 m, and the observation is smoothed with a Hanning window having a Full Width at Half Maximum (FWHM) of $\Delta_{z_{\mathrm{smooth}}}$ = 620 m. Temporal integration is Δ_t = 80 s, with boxcar smoothing to FWHM $\Delta_{t_{\mathrm{smooth}}}$ = 400 s.

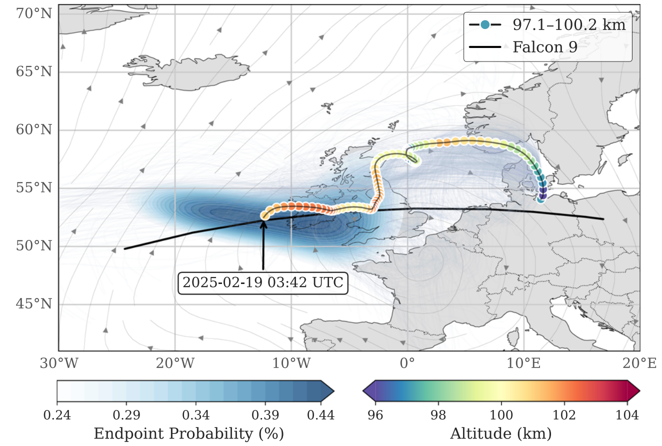

Fig. 3 | Plausible back-trajectories linking Falcon 9 to lithium observation. A set of randomly perturbed back trajectories of the lithium plume from Kühlungsborn, calculated using winds from the UA-ICON model. The probability density heat map shows endpoints of many trajectories (blue) terminating in the region corresponding to the most likely origin of the lithium plume. One plausible back trajectory (coloured circles, colour indicates altitude) began at 00:21 UTC on 20 February over Kühlungsborn (54°N, 12°E) at an altitude of 97.1 km, and terminated at the Falcon 9 re-entry time, 03:42 UTC on 19 February, west of Ireland at (52.5°N, 12.38°W) and an altitude of 100.2 km. The best estimate for the Falcon 9 re-entry trajectory (courtesy of the European Space Agency) is plotted for comparison (black).

Based on the arrival time of the lithium plume in the lidar observation, and supported by coincident measurements of the local three-dimensional wind field from our Spread spectrum Interferometric multistatic Meteor radar Observing Network (SIMONe-Germany), we hypothesised that the plume might be linked to the Falcon 9 re-entry event. To support this hypothesis, we sought to answer the following questions:

1. Does a lithium plume back trajectory intersect the Falcon 9 re-entry trajectory?
2. Can we exclude natural processes as the source of the elevated lithium?

Does the Li plume back trajectory intersect Falcon 9?

We used UA-ICON to simulate the possible back trajectories of the lithium plume. We ran 8000 randomly perturbed back trajectories using the measured wind variability from the radar to introduce realistically scaled perturbations in each of the three wind components of the UA-ICON output. The set of calculated trajectories (blue) is shown in Fig. 3 with a probability density heatmap showing the region over the UK and Ireland where the lithium plume likely originated. The re-entry trajectory of Falcon 9 provided by the European Space Operations Centre (black) passed through this region. One example back trajectory (filled circles, colours indicate altitude) begins above Northern Germany at 97.1 km at 00:21 UTC, near the peak lithium density observed by the lidar at Kühlungsborn, and terminates off the west coast of Ireland at 100.2 km at 52.5°N, 12.38°W, consistent with the Falcon 9 re-entry time of approximately 03:42 UTC. The temporal intersection between the UA-ICON back trajectory and the Falcon 9 re-entry path has a spatial separation of less than 2 km vertically and less than 10 km horizontally.

Back trajectories starting at other altitudes in the thermosphere and lower mesosphere do not terminate over the UK and Ireland. The air sampled by the lidar between 96 and 97.5 km did not originate from elsewhere in Europe or experience large vertical advection.

Can natural sources for the Li plume be reasonably excluded?

Metallic ion layers are a natural feature of the ionospheric E-region (90–130 km) and are frequently observed in association with sporadic E-layers (Es). These Es layers are thought to form through the wind shear-driven convergence of metallic ions such as Fe$^+$, Mg$^+$, and Ca$^+$. The formation of an Es layer via vertical shear of the horizontal wind, followed by downward transport by the diurnal tide, and higher harmonics, to below 100 km, and subsequent neutralisation of the metal ions, can produce a layer of enhanced neutral metal atoms[16].

Sporadic E layers are routinely measured using a nearby ionosonde at Juliusruh, approximately 116 km east of the lidar and radar at Kühlungsborn. In the upper panel of Fig. 4, no pronounced electron enhancement (foEs) is visible in the 4.5 hours preceding the observed lithium plume. Sporadic E layers earlier on 19 February were weak and unremarkable. The coloured contours in the figure represent the vertical shear of the magnetic-eastward wind at the ionosonde, as measured by SIMONe-Germany. Negative vertical shear (orange) of the magnetic-eastward wind corresponds to positive vertical ion convergence, which is a favourable condition for the formation of Es layers[17].

The middle panel of Fig. 4 provides additional context for the lithium observation by presenting concurrent wind shear measurements at the lidar location. In this case, the lithium plume is situated within a region of weak positive wind shear (blue), which does not favour ion convergence and layer formation.

The lower panel of Fig. 4 displays the geomagnetic activity, as indicated by the local K index derived from observations of the Juliusruh geomagnetic station. Periods of high geomagnetic activity ($K > 5$) could signal a storm of sufficient intensity to perturb the MLT through Joule heating, particle precipitation, or variations in the electric field. Such disturbances can impact neutral dynamics and may promote the formation of convergent shear layers, as discussed above[18]. In the present case, there is no indication of a significant geomagnetic storm that could enhance the likelihood of forming a neutral atomic lithium layer via downward convergence of ionic Li$^+$ from the thermosphere.

In summary, the three panels of Fig. 4 show no enhanced foEs preceding the observation of the Li plume, relatively weak vertical shear in the horizontal winds, and no geomagnetic activity that would likely lead to the formation of the observed neutral Li layer at 96 km. Quantitative climatological support for this claim is presented in Fig. 1 of the Supplementary Information.

Discussion

The Falcon 9 case study on 19 February 2025 is both a harbinger of the expected increase in the number of satellite and rocket re-entry events over

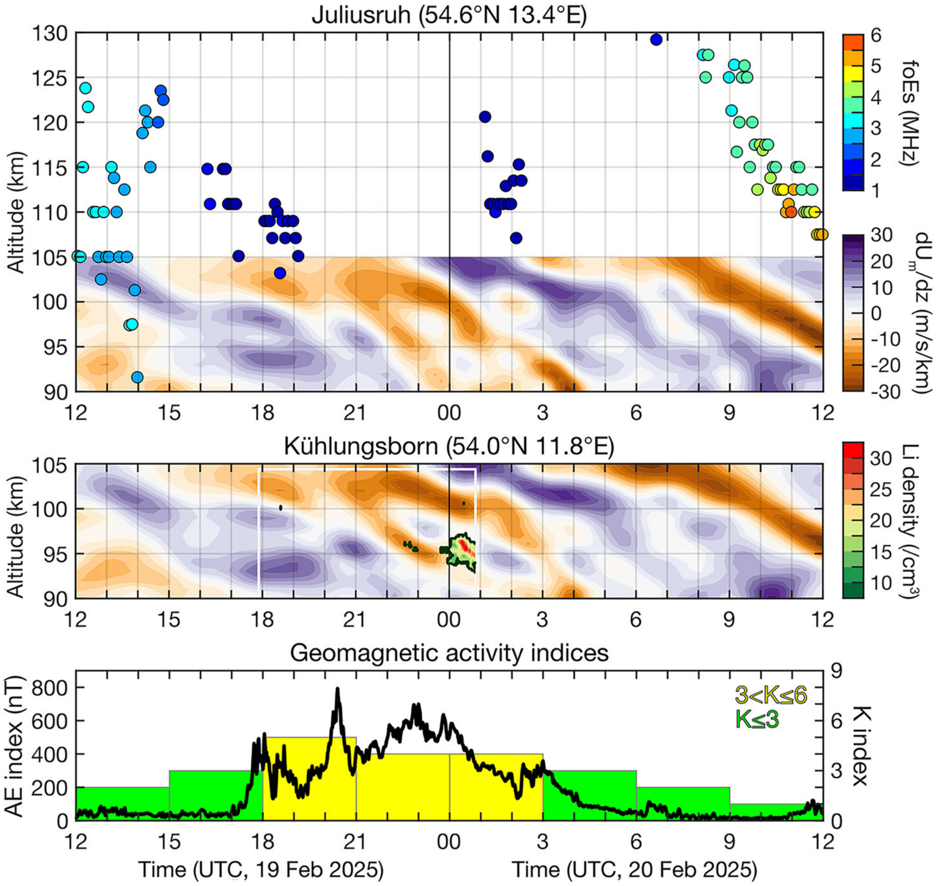

Fig. 4 | Ionospheric observations supporting the anthropogenic origin of the lithium plume. The upper panel shows the SIMONe-observed wind shear at Juliusruh (54.6°N,13.4°E) overlayed with the co-located ionosonde observations, the middle panel shows the SIMONe-observed wind shear at Kühlungsborn (54.0°N,11.8°E) overlayed with the lidar measurements.

the coming decade and an excellent test of our ability to monitor and detect the pollution which results from the re-entry of artificial satellites.

The lidar observation of a transient, high-density lithium plume at 96 km over Kühlungsborn represents the first time- and altitude-resolved measurement of pollution after re-entry of space debris. The timing, altitude, and density of the observed lithium plume, combined with the back trajectory analysis using UA-ICON winds and the known re-entry of the Falcon 9 upper stage, provide strong evidence linking this plume to the ablation of engineered materials during atmospheric re-entry. This work represents the first demonstration of back trajectory calculations using upper atmospheric horizontal winds from UA-ICON, supported by measured variances from the radar. The success of these back trajectory calculations from Kühlungsborn to the rocket re-entry point is a milestone achievement for upper-atmospheric modelling.

These unique measurements demonstrate that ablation of spacecraft components, particularly those containing aluminium, begins as high as 100 km altitude. This conclusion supports recent work, conducted in the lower stratosphere, attributing significant middle-atmospheric pollution to space debris[2,6,8]. Our observations of lithium at 96 km should be interpreted as a lower limit, since some fraction of lithium atoms will be converted to molecular forms below 95 km, and Li^+ ions above 100 km en route to Northern Germany. We also expect that the majority of the 30 kg of lithium present in the Falcon 9 is vaporised at altitudes well below 100 km where measurements are not possible because the Li atoms are immediately oxidised to LiO and LiO_2. However, measuring trace amounts of lithium from space debris pollution in the MLT, using remote sensing by lidar, can inform estimates of atmospheric metallicity at lower altitudes. In this way, lithium may act as a sentinel or tracer element, signalling the broader presence of other metallic species descending into the stratosphere.

Alternative explanations for the formation of a neutral lithium layer, such as downward transport from metallic ion layers associated with sporadic E events, appear unlikely. Ionograms from the nearby Juliusruh ionosonde show no significant enhancement in electron density in the hours surrounding the lidar detection, and meteor radar measurements do not reveal shear structures consistent with Es-related convergence at the relevant altitudes. Furthermore, geomagnetic conditions remained relatively quiet during the observation window, reducing the likelihood of storm-driven neutral layer formation. Climatological data for both the ionosonde and radar are given in Figs. 2 and 3 of the Supplementary Information and show that the lithium observation occurred under climatologically expected conditions.

Environmental concerns about re-entering space debris have primarily focused on potential catalytic effects of aluminium and other metals on the stratospheric ozone layer. However, detecting and quantifying pollutants in this region is technically challenging and expensive. The upper atmosphere, as the first part of the Earth's environment impacted by re-entry, offers a valuable opportunity to observe ablated materials close to their source, before they undergo chemical transformation and atmospheric dispersion. The detection of lithium presented here highlights the diagnostic potential of resonance fluorescence lidar, especially when combined with other atmospheric measurements and supported by model analysis. Expanding such observational capabilities, both in geographical coverage and to other elemental species, will be essential for assessing the long-term consequences of space debris pollution on the Earth's atmosphere.

Beyond this single event, recurring re-entries may sustain an increased level of anthropogenic flux of metals and metal oxides into the middle atmosphere with cumulative, climate-relevant consequences. After oxidation and heterogeneous uptake on alumina and other metal-oxide particles, aluminium and co-injected species could perturb stratospheric ozone chemistry, modify high-altitude aerosol microphysics through new particle formation, growth, and coagulation, and thereby influence radiative balance. Key unknowns include emission inventories for rockets and satellites, lack of a systematic observational survey of mesospheric metals, altitude-time ablation profiles, chemical lifetimes, particle size-composition distributions, and transport pathways into the lower stratosphere. Addressing these uncertainties will require coordinated, multi-site observations (including resonance-fluorescence and elastic lidars, in situ sampling, and satellites), together with whole-atmosphere chemistry-climate modelling to connect event-scale injections to long-term impacts.

Methods

Lithium resonance fluorescence lidar

Observations of mesospheric lithium were conducted using a metal resonance fluorescence lidar system tuned to the ground-state atomic transition of lithium at 670.9778 nm (vacuum), 670.7926 nm (air). The system employs a 50 Hz xenon-chloride (XeCl) excimer laser to pump a dye solution, specifically 4-(Dicyanomethylene)-2-methyl-6-(4-dimethylaminostyryl)-4H-pyran (DCM), dissolved in propylene carbonate. The resulting laser wavelength is monitored continuously using a wavemeter from Bristol Instruments (model 871A) to ensure frequency stability, better than 0.0001 nm throughout the measurement period.

The average laser output energy was approximately 5 mJ and the beam divergence is 0.5 mrad. A beam expander is used to reduce divergence so that the laser illuminates a spot of approximately 100 m diameter at an altitude of 100 km. The transmitted beam is directed vertically.

Backscattered photons are collected by a receiving telescope with an aperture of 78 cm and guided by quartz fibre to the detectors. Spectral filtering is achieved with an interference filter centred at 670.8 ± 1.3 nm (air), used to suppress sky background. The filter is on an optical table in a climate-controlled room.

Detection is performed using an avalanche photodiode (APD). The signal is integrated with a vertical resolution of 200 m and smoothed using a Hanning window with FWHM of 620 m. Temporal integration is 80 s per profile with a boxcar smoothing window with FWHM of 400 s.

The lidar system has previously been used for resonance fluorescence observations of calcium[19] and nickel[20], demonstrating its applicability to multi-element detection of mesospheric metals. Further technical details, uncertainty budgets, and initial measurements of lithium with our lidar can be found in ref. 21.

Radar wind measurements

To investigate wind dynamics in the Mesosphere and Lower Thermosphere (MLT), we used a radar-based technique that detects the motion of meteoric trails formed as interplanetary dust particles ablate upon entering Earth's atmosphere. These short-lived plasma trails act as coherent reflectors of radio waves, enabling remote sensing of neutral winds at altitudes between approximately 80 and 100 km.

The fundamental observable is the Doppler shift f of the backscattered signal, which reflects the projection of the local wind vector $\vec{u}$ onto the Bragg wave vector $\vec{k}$, plus a random measurement error ξ[22,23]:

$$2\pi f = \vec{u} \cdot \vec{k} + \xi \tag{1}$$

By combining Doppler measurements from multiple viewing geometries, it is possible to reconstruct the full three-dimensional wind vector $\overrightarrow{u}$, typically expressed in an east-north-up (ENU) coordinate system as zonal (u), meridional (v), and vertical (w) components.

For this work, wind measurements were obtained using the SIMONe-Germany system[24], a coherent multi-static system operated by the Leibniz Institute of Atmospheric Physics and centred near Kühlungsborn (53°N, 12.5°E). The network operates at 32.55 MHz and consists of two transmitting sites (each with six antennas) and seven remote receiving stations. Five of the receivers use a single dual-polarised antenna, while two are equipped with arrays of five dual-polarised antennas. This configuration enables high meteor detection rates and precise multi-angle triangulation of meteor trail positions and velocities across northern Germany.

To derive continuous wind fields from these sparse detections, we applied the HYPER framework (HYdrodynamic Point-wise Environment Reconstructor[25]), a physics-informed neural network that infers four-dimensional wind fields (latitude, longitude, altitude, and time). HYPER incorporates both mass and momentum conservation as soft constraints and employs spatial regularisation to ensure physical consistency. This approach is especially effective in regions with sparse sampling, yielding dynamically coherent wind estimates.

The resulting wind fields span 19-20 February 2025, with a temporal resolution of 15 minutes, vertical resolution of 1 km, and horizontal grid spacing of approximately 0.2° in latitude and 0.3° in longitude. These data were used to evaluate the accuracy of the UA-ICON model and to define perturbation amplitudes in the ensemble back-trajectory simulations described in Section "Measurement of a lithium plume by lidar". In addition, the wind fields were analysed for the presence of vertical wind shears, as shown in Fig. 4.

UA-ICON Global Circulation Model

The Upper Atmosphere ICON (UA-ICON) model is a high-top extension of the ICON general circulation model, developed to simulate the dynamics of the entire atmosphere from the surface up to the lower thermosphere. In this study, we use UA-ICON outputs with a horizontal resolution of 20 km and a vertical domain extending to 150 km, providing 10-minute wind fields suitable for trajectory calculations in the mesosphere and lower thermosphere (MLT). The large-scale dynamics were specified by nudging to ECMWF operational analyses up to an altitude of 50 km, ensuring the model remains as close as possible to the observations in the troposphere and lower stratosphere. The model includes non-hydrostatic dynamics, realistic orography, and parameterisations for gravity wave drag and eddy diffusion, enabling a reliable representation of atmospheric circulation up to ~ 150 km[26].

The back trajectories were calculated on an interpolated UA-ICON dataset using a Runge-Kutta integration scheme. The measured 1σ variability at 90 km in the radar wind field during this time is used to scale the random perturbations in the UA-ICON back trajectories. The radar measured wind variabilities of 18 m/s for the zonal wind, 26 m/s for the meridional wind, and 0.5 m/s for the vertical wind. A comparison of horizontal winds in UA-ICON and winds measured by the SIMONe Germany meteor radar is shown in Figs. 4, 5, and 6 of the Supplementary material.

Juliusruh ionosonde measurements

Sporadic E layer activity was monitored using data from the Juliusruh ionosonde, located at 54.6°N, 13.4°E on the Baltic Sea coast of Northern Germany. The station provides continuous (5-minute integration), high-resolution measurements of ionospheric plasma frequency and is part of a long-term monitoring effort of ionospheric variability in Europe[27].

In this study, foEs denotes the maximum plasma frequency (in MHz) at which radio waves are reflected from the Es layer, serving as a proxy for electron density and hence sporadic metal layer formation. Typical foEs values range from 2 to 10 MHz, with the upper end corresponding to strongly ionised layers.

Geomagnetic indices

The K index is a 3-hourly index of local geomagnetic activity[28]. We use the K index derived from geomagnetic field measurements at Juliusruh (54.6°N, 13.4°E). The index ranges from 0 to 9 in increments of 1. Values larger than 5 may be regarded as possible geomagnetic storms.

The auroral electrojet (AE) index represents the strength of the auroral electrojet[29]. The index is based on geomagnetic field measurements around the auroral oval. The AE index has a temporal resolution of 1 minute, which allows it to capture shorter-period variations than the K index. Values exceeding 1000 nT may be considered as strong geomagnetic substorms[30].

Leeds chemical ablation model

The ablation model describes a sheet of material entering the atmosphere in a direction orthogonal to the plane of the sheet, and with no significant rotation. The thickness of the sheet is much smaller than its planar dimensions. The model treats a small cylindrical unit in the middle of the sheet, with a radius r (typically $r = 400\,\mu$m) and length equal to the sheet width (set to between 0.1 cm and 5 cm). One end of the cylinder is at the leading side of the sheet, where collisions with air molecules cause heating and ablation. The opposite end of the cylinder does not undergo collisional heating, but can radiate heat conducted through the cylinder from the leading edge, and also undergo ablation.

The model assumes a negligible temperature gradient, and hence negligible heat transfer, between the cylinder and the rest of the sheet (because the planar dimensions of the sheet are large compared with its thickness, minimising edge effects). Because the thermal conductivity of Al is unusually large ($\kappa = 237$ W m^{-1} K^{-1}[31]), there is rapid heat transfer along the axis of the cylinder from the leading to the trailing side of the sheet. This means the heating of the cylinder is close to isothermal: even for a thickness of 50 cm, the Biot number remains below the threshold of 0.1[32].

The classical meteor equations used in the Leeds Chemical Ablation Model[11] are modified to treat the entry of the cylinder. Conservation of momentum yields:

$$\frac{dV}{dt} = -\Gamma \pi r^2 V^2 \frac{\rho_a}{m} + g \tag{2}$$

where V is the velocity of the sheet, ρ_a is the mass density of the atmosphere, m is the mass of the cylinder, and g is gravitational acceleration. The dimensionless free-molecular drag coefficient Γ, describing momentum transfer efficiency, is typically set to 1.

The rate of ablative mass loss from a pure Al surface is:

$$\frac{dm}{dt} = \gamma p_{\mathrm{Al}} \pi r^2 \sqrt{\frac{m_{\mathrm{Al}}}{2\pi k_B T}} \tag{3}$$

where γ is the uptake coefficient (set to 1), p_{Al} is the equilibrium vapour pressure of Al[31], and m_{Al} is the atomic mass of Al.

To treat thermal diffusion along the cylinder axis z, the cylinder is divided into n segments of width ∂z. For segment 1 at the leading edge, energy conservation yields:

$$\begin{aligned}\frac{1}{2}\pi r^2 V^3 \rho_a \Lambda &= \pi r^2 \varepsilon\sigma\left(T_1^4 - T_{\mathrm{env}}^4\right) + \left(\pi r^2 \partial z\right)\rho_m C \frac{dT_1}{dt} \\ &\quad + L\frac{dm_1}{dt} + \kappa\frac{T_1 - T_2}{\partial z}\end{aligned} \tag{4}$$

The left-hand side describes collisional heating, where Λ (set to 1) is the heat transfer coefficient. The right-hand side terms represent radiative loss (with $\varepsilon = 1$, σ the Stefan-Boltzmann constant, and $T_{\mathrm{env}} = 200$ K), thermal heating, ablation, and thermal diffusion.

The additional parameters are:

- $\rho_m = 2700$ kg m^{-3}
- Melting point = 933 K
- Latent heat of sublimation, $L = 1.09 \times 10^7$ J kg^{-1}
- Specific heat capacity, $C = 893$ J K^{-1} kg^{-1}[31]

Equation (4) can be rearranged to yield the rate of temperature change of segment 1. For an intermediate segment i, the temperature evolution is:

$$\frac{dT_i}{dt} = \frac{\kappa\left(T_{i-1} - T_{i+1}\right)dz}{C\left(\pi r^2 \partial z\right)\rho_m} \tag{5}$$

For the final segment, which undergoes heat loss through ablation and radiation, $\frac{dT_n}{dt}$ is computed similarly, but without the collisional heating term.

Figure 5 shows the expected ablation altitudes for rockets with aluminium hulls of various thicknesses. This figure uses a re-entry angle of 88.8° from zenith, as estimated from the Falcon 9 trajectory. A shallow re-entry angle increases the path length through the atmosphere, resulting in a slower heating rate because there is a lower rate of collisions with air molecules, and the object has more time to lose heat through radiation. Nevertheless, the melting point of the material is still reached at a higher altitude, producing an extended near-horizontal ablation trail. In contrast, a steep re-entry angle produces rapid deceleration and intense heating, but the ablation occurs at lower altitudes with less lateral dispersion of debris.

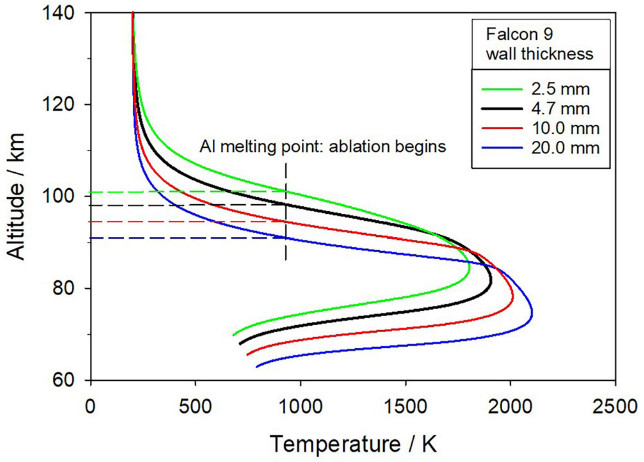

Fig. 5 | Ablation profiles for aluminium rockets. The expected ablation profiles for rockets with aluminium hulls of various thicknesses. Derived using the Leeds Chemical Ablation Model, assuming a shallow re-entry angle of 88.8° to zenith. The Falcon 9 is reported to have a hull thickness of 4.7 mm and should reach a melting temperature of 933 K at 98.2 km.

Communication with SpaceX

Prior to publication of this manuscript, we contacted Space Exploration Technologies Corp. (SpaceX) and provided the full article, a summary of our analysis, and the underlying data, inviting comments and corrections. No response had been received at the time of acceptance.

Generation of Figure 1

Figure 1 was generated using the *KDE Marble*[33] virtual globe (Atlas theme), which utilises Micro World Data Bank II[34] coastline and boundary data and Shuttle Radar Topography Mission (SRTM) elevation data[35]. SRTM data are courtesy of the National Aeronautics and Space Administration (NASA) and the National Geospatial-Intelligence Agency (NGA). The final layout and annotations were produced in *LibreOffice Draw*[36]. The satellite and combustion-plume symbols were illustrated by João Maia, PhD.

Data availability

All data used in the production of the figures in this study is stored in a repository with the following DOI: 10.22000/gdp71mh7gm8ufks6.

Code availability

The UA-ICON source code for version ua-icon-2.1 is published on Zenodo (Kunze et al., 2024), £ https://doi.org/10.5281/zenodo.13927891. It is based on the ICON open source release (ICON partnership (DWD, MPI-M, DKRZ, KIT, and C2SM), 2024), ICON release 2024.01. World Data Center for Climate (WDCC) at DKRZ. https://doi.org/10.35089/WDCC/IconRelease01, which is available under a BSD 3-clause license (see https://www.icon-model.org, accessed June 2025). The code to calculate the ensemble back-trajectories is publicly available at https://github.com/deterministic-nonperiodic/lagrangian_trajectories.git. The HYPER code is publicly available on GitHub via Zenodo: https://doi.org/10.5281/zenodo.12671264.

Received: 22 July 2025; Accepted: 19 December 2025;
Published online: 19 February 2026

References

1. Caleb Henry. SpaceX submits paperwork for 30,000 more Starlink satellites. https://spacenews.com/spacex-submits-paperwork-for-30000-more-starlink-satellites/ (2019). Accessed: 2025-05-10.
2. Schulz, L. & Glassmeier, K.-H. On the anthropogenic and natural injection of matter into Earth's atmosphere. *Adv. Space Res.* **67**, 1002–1025 (2021).
3. Lodders, K., Bergemann, M. & Palme, H. Solar System elemental abundances from the solar Photosphere and CI-Chondrites. *Space Sci. Rev.* **221**, 23 (2025).
4. Lodders, K. Solar System abundances and Condensation Temperatures of the elements. *Astrophysical J.* **591**, 1220–1247 (2003).
5. Ferreira, J. P., Huang, Z., Nomura, K. -i & Wang, J. Potential ozone depletion from satellite demise during atmospheric reentry in the era of mega-constellations. *Geophys. Res. Lett.* **51**, e2024GL109280 (2024).
6. Boley, A. C. & Byers, M. Satellite megaconstellations create risks in Low Earth Orbit, the atmosphere and on Earth. *Sci. Rep.* **11**, 10642 (2021).
7. Ryan, R. G., Marais, E. A., Balhatchet, C. J. & Eastham, S. D. Impact of rocket launch and space debris air pollutant emissions on stratospheric Ozone and global Climate. *Earth's. Future* **10**, e2021EF002612 (2022).
8. Murphy, D. M. et al. Metals from spacecraft reentry in stratospheric aerosol particles. *Proc. Natl. Acad. Sci.* **120**, e2313374120 (2023).
9. Maloney, C. M., Portmann, R. W., Ross, M. N. & Rosenlof, K. H. Investigating the potential atmospheric accumulation and radiative impact of the coming increase in satellite reentry frequency. *J. Geophys. Res.: Atmospheres* **130**, e2024JD042442 (2025).
10. Shareefdeen, Z. & Al-Najjar, H. Pollution effects and management of orbital space debris. *ACS Omega* **9**, 5127–5141 (2024).
11. Vondrak, T., Plane, J. M. C., Broadley, S. & Janches, D. A chemical model of meteoric ablation. *Atmos. Chem. Phys.* **8**, 7015–7031 (2008).
12. Jegou, J.-P., Chanin, M.-L., Mégie, G. & Blamont, J. E. Lidar measurements of atmospheric lithium. *Geophys. Res. Lett.* **7**, 995–998 (1980).
13. Asplund, M., Grevesse, N., Sauval, A. J. & Scott, P. The chemical composition of the Sun. *Annu. Rev. Astron. Astrophys.* **47**, 481–522 (2009).
14. Carrillo-Sánchez, J. D. et al. Cosmic dust fluxes in the atmospheres of Earth, Mars, and Venus. *Icarus* **335**, 113395 (2020).
15. Wanhill, R. & Bray, G. Chapter 2 - Aerostructural design and its application to aluminum-lithium alloys. In *Aluminum-lithium Alloys* (eds Eswara Prasad, N., Gokhale, A. A. & Wanhill, R.) 27–58 (Butterworth-Heinemann, Boston, 2014).
16. Cox, R. M. & Plane, J. M. C. An ion-molecule mechanism for the formation of neutral sporadic Na layers. *J. Geophys. Res.: Atmospheres* **103**, 6349–6359 (1998).
17. Yamazaki, Y. et al. Examining the wind shear theory of sporadic e with icon/mighti winds and cosmic-2 radio occultation data. *Geophys. Res. Lett.* **49**, e2021GL096202 (2022).
18. Plane, J. M. C., Feng, W. & Dawkins, E. C. M. The Mesosphere and Metals: Chemistry and changes. *Chem. Rev.* **115**, 4497–4541 (2015).
19. Gerding, M., Alpers, M., von Zahn, U., Rollason, R. J. & Plane, J. M. C. Atmospheric Ca and Ca^+ layers: Midlatitude observations and modeling. *J. Geophys. Res.: Space Phys.* **105**, 27131–27146 (2000).
20. Gerding, M., Daly, S. & Plane, J. M. C. Lidar soundings of the mesospheric nickel layer using Ni(^{3}F) and Ni(^{3}D) transitions. *Geophys. Res. Lett.* **46**, 408–415 (2019).
21. Gerding, M., Wing, R., Feng, W., Plane, J. M. C. & Baumgarten, G. New Li lidar observations and model simulations: A window to anthropogenic signatures. *Geophys. Res. Lett.* **52**, e2025GL118710 (2025).
22. Hocking, W. K., Fuller, B. & Vandepeer, B. Real-time determination of meteor-related parameters utilizing modern digital technology. *J. Atmos. Sol.-Terrestrial Phys.* **63**, 155–169 (2001).
23. Holdsworth, D. A., Reid, I. M. & Cervera, M. A. Buckland Park all-sky interferometric meteor radar. *Radio Sci.* **39**, RS5009 (2004).
24. Chau, J. L. et al. Novel specular meteor radar systems using coherent MIMO techniques to study the Mesosphere and Lower Thermosphere. *Atmos. Meas. Tech.* **12**, 2113–2127 (2019).
25. Urco, J. M., Feraco, F., Chau, J. L. & Marino, R. Augmented four-dimensional Mesosphere and Lower Thermosphere wind field reconstruction via the physics-informed machine learning approach HYPER. *J. Geophys. Res.: Mach. Learn. Comput.* **1**, e2024JH000162 (2024).
26. Kunze, M. et al. UA–ICON with NWP physics package (version: ua-icon-2.1): Mean state and variability of the middle atmosphere. *Geoscientific Model Dev. Discuss.* **2024**, 1–41 (2024).
27. Sivakandan, M. et al. Long-term variations and residual trends in the E, F, and sporadic E (Es) layer over Juliusruh, Europe. *J. Geophys. Res.: Space Phys.* **128**, e2022JA031097 (2023).
28. Matzka, J., Stolle, C., Yamazaki, Y., Bronkalla, O. & Morschhauser, A. The geomagnetic Kp index and derived indices of geomagnetic activity. *Space Weather* **19**, e2020SW002641 (2021).
29. Davis, T. N. & Sugiura, M. Auroral electrojet activity index AE and its universal time variations. *J. Geophys. Res.* **71**, 785–801 (1966).
30. Zong, Q.-G., Yue, C. & Fu, S.-Y. Shock induced strong substorms and super substorms: Preconditions and associated oxygen ion dynamics. *Space Sci. Rev.* **217**, 1–34 (2021).
31. Lide, D. R. (ed.) *CRC Handbook of Chemistry and Physics* (CRC Press, Boca Raton, FL, 2006).
32. Yener, Y. & Kakac, S. *Heat Conduction* (CRC Press, Boca Raton, 2018). https://doi.org/10.1201/9780203752166.
33. KDE e.V. *Marble Virtual Globe*. KDE (2025). https://marble.kde.org. Version X.Y, Atlas theme, accessed 2025-12-11.
34. Micro Doc. Micro World Data Bank II: Coastlines, Country Boundaries, Islands, Lands, and Rivers (1988). Cartographic dataset.
35. Farr, T. G. et al. The Shuttle Radar Topography Mission. *Rev. Geophysics* **45**, RG2004 (2007).
36. The Document Foundation. *LibreOffice Draw* (2025). https://www.libreoffice.org/discover/draw/. Version X.Y, accessed 2025-12-11.

Acknowledgements

We thank Mr. Michael Priester for technical support on the lidar instrumentation. We would like to thank Mr. Stijn Lemmens and Dr. Silvia Sanvido at the European Space Operations Centre for providing the Falcon 9 re-entry trajectory. This work used resources of the Deutsches Klimarechenzentrum (DKRZ) granted by its Scientific Steering Committee (WLA) under project ID bm1233. C.C.S. is funded by the Leibniz Competition through the project IMPAGT (P160/2023). Y.A.M. received support through Schmidt Sciences, LLC., as part of the Virtual Earth System Research Institute (VESRI). J.M.C.P. was supported by the European Space Agency and UK Space Agency (EISI agreement 4000146844).

Author contributions

R.W. made the lidar observation, collected and organised the data for the study, solicited expertise from co-authors, and wrote the initial manuscript. M.G. calibrated the lidar, processed the lithium data, and provided critical editing. J.M.C.P. provided model results for the ablation altitude of Falcon 9 as well as estimates of natural lithium injection. Y.A.M. set up and ran the UA-ICON model and calculated back trajectories. J.M.U. produced 3D radar winds used in the study. Y.Y. and C.S. conducted the analysis, which excludes natural sources for the lithium plume. L.S. conducted the analysis to estimate the mass ablated from Falcon 9 and advected in the plume. J.H. provided scientific advice on the interpretation of the lithium layer. J.M. scaled and provided the Ionosonde data. T.R. provided access to the radar

winds. C.C.S. provided access to software and resources for a dedicated UA-ICON simulation. G.B. provided initial camera observations of the re-entry, scientific insight, and critical editing. All authors contributed to the final version of the manuscript.

Competing interests

The authors declare no competing interest.

Additional information

Supplementary information The online version contains supplementary material available at https://doi.org/10.1038/s43247-025-03154-8.

Correspondence and requests for materials should be addressed to Robin Wing.

Peer review information *Communications Earth & Environment* thanks Paytsar Muradyan, Rolf Rüfenacht and the other, anonymous, reviewer(s) for their contribution to the peer review of this work. Primary Handling Editors: Mengze Li and Joe Aslin. [A peer review file is available].

Reprints and permissions information is available at http://www.nature.com/reprints

Publisher's note Springer Nature remains neutral with regard to jurisdictional claims in published maps and institutional affiliations.

Open Access This article is licensed under a Creative Commons Attribution 4.0 International License, which permits use, sharing, adaptation, distribution and reproduction in any medium or format, as long as you give appropriate credit to the original author(s) and the source, provide a link to the Creative Commons licence, and indicate if changes were made. The images or other third party material in this article are included in the article's Creative Commons licence, unless indicated otherwise in a credit line to the material. If material is not included in the article's Creative Commons licence and your intended use is not permitted by statutory regulation or exceeds the permitted use, you will need to obtain permission directly from the copyright holder. To view a copy of this licence, visit http://creativecommons.org/licenses/by/4.0/.

© The Author(s) 2026